https://doi.org/10.5194/egusphere-2024-3645
Preprint. Discussion started: 3 January 2025

Modeling Total Phosphorus Transport in the European Riverine System: Parameterization and Projections under Climate and Socioeconomic Scenarios

Alberto Elizalde[1], Gibran Romero-Mujalli[2,3], Tobias Stacke[4], and Stefan Hagemann[1]

[1]Institute of Coastal Systems, Analysis and Modelling, Helmholtz-Zentrum Hereon, Geesthacht, Germany.
[2]Institute for Geology, University of Hamburg, Germany.
[3]Penpet Petrochemical Trading GmbH, Hamburg, Germany.
[4]Max Planck Institute for Meteorology, Hamburg, Germany.

Correspondence: Alberto Elizalde (alberto.elizalde@hereon.de)

Abstract.

Eutrophication is recognized as a critical ecological challenge that detrimentally affects aquatic ecosystems in both riverine and marine environments. Understanding how future human actions may influence nutrient pollution is crucial for mitigating these effects. While studies have focused on phosphorus trends related to fertilizer use in cropland areas only, this study also considers land-use changes and human development as defined by the Shared Socioeconomic Pathways (SSPs). Phosphorus transport trends are estimated using a new parameterization in a hydrological model, taking into account the evolution of agricultural, urban, and natural land use types, in line with the SSP narratives, as well as aquaculture activities, atmospheric deposition, and weathering process. Additionally, the effects of global warming are integrated by incorporating simulated hydrological data following three Representative Concentration Pathways scenarios. Total phosphorus load budgets are estimated for the four semi-enclosed European seas. The findings indicate that phosphorus losses are primarily driven by human development and land-use expansion, outweighing the response from pollution control policies and technological advances and, to some extent, hydrological changes due to climate change. The scenario data generated, and the new parameterization implemented within an Earth system model framework, can serve as a valuable resource for ecosystem modeling efforts.

1 Introduction

Human activities exert significant impacts on ecosystems, often contributing negatively to environmental and climatic conditions. A key example is eutrophication, driven by excessive fertilizer use in agriculture, urban runoff and wastewater, which results in significant nutrient runoff that disrupts the natural phosphorus cycle and detrimentally affects aquatic ecosystems in both, riverine and marine environments (Smith et al., 2006; Yuan et al., 2018). Understanding how future human activities might influence nutrient pollution in rivers and its subsequent discharge into the ocean is essential for anticipating and mitigating such impacts.

Nutrient excess particularly from agricultural fertilizer applications are widely recognized as a significant contributor to eutrophication in aquatic systems. The influx of nutrients from croplands into water bodies promotes rapid growth of plants

https://doi.org/10.5194/egusphere-2024-3645
Preprint. Discussion started: 3 January 2025

and algae, leading to localized oxygen depletion and the development of hypoxic or anoxic conditions, which in turn reduces the population of larger aquatic organisms (Devlin and Brodie, 2023). Research on nutrient pollution has primarily focused on changes in the global nitrogen (N) cycle, the impact of human activities on the global phosphorus (P) cycle, which has been significantly disrupted in recent decades, has received comparatively less attention (Yuan et al., 2018).

It has been estimated that from the total phosphorus (TP) applied, P losses from cropland areas account for about 50-60% globally and up to 80% in industrialized countries (Kronvang et al., 2007; Alewell et al., 2020; Bayad et al., 2022). Despite the relevance of the ecological problem, the quantities of P losses into rivers remains highly uncertain. Part of the problem is to quantify losses from croplands through different pathways, such as runoff, leaching and soil erosion, into river systems. The variability in the results of previous studies is largely due to the wide range of conditions under which the studies were conducted, e.g. topography of agricultural plots, meteorological conditions, fertilizer type and management, etc. (Hart et al., 2004; Alewell et al., 2020). Furthermore, the limited number of observations at river stations and the relatively short temporal coverage limit the overall estimate of TP discharged at river mouths.

Efforts have been made to estimate the future usage and associated losses of nutrients. Previous studies have pointed out that future projections of phosphorus demand will increase due to cropland expansion policies according to the Shared Socioeconomic Pathways (SSPs) (Mogollón et al., 2018, 2021). Moreover, Liu et al. (2020) investigated trends in global phosphorus losses from cropland areas under future climate projections according to the future Representative Concentration Pathways (RCP) scenarios. They concluded that estimated P losses from cropland areas are projected to increase by 16 and 31% by the end of the century (2080-2099) in the RCP 2.6 and 8.5 scenarios, respectively, compared to the 1991-2010 baseline, driven solely by the rise in annual precipitation. Bouwman et al. (2011) also found a positive trend in nutrient surplus estimates for future global changes. They used the International Assessment of Agricultural Knowledge, Science and Technology for Development scenario (IAASTD) to conclude that globally phosphorus surplus will increase by 54% in the year 2050 compared to the 1900-1950 baseline.

This study aims to comprehensively quantify TP losses from land to sea, taking into account the combined effects of socio-economic and climate change factors. Given the prevalence of eutrophication in industrialised regions, the research focuses on European areas, in particular on phosphorus load budgets of semi-enclosed seas. The methodology integrates estimates of TP inputs into the riverine system, i.e. it considers not only P losses from cropland but also includes contributions from weathering, erosion, atmospheric deposition, and losses from natural lands and anthropogenic sources such as agriculture, pasture, aquaculture, and urban wastewater. The related P concentrations are based on data obtained from the IMAGE-GNM model (Beusen et al., 2015), which has been utilized to develop socio-economic scenarios of the SSP narratives (Hurtt et al., 2020). This dataset serves as a baseline for historical reference values.

To model TP transport, we employ the Hydrological Discharge (HD) model (Hagemann et al., 2020) to estimate catchment-scale lateral P loads from land areas into the rivers and to route these fluxes to the river mouths. Due to the lack of explicit P concentration data in future scenarios, a new scheme was developed to parameterize P losses from agricultural sources based on N data from fertilizer application information and land-use cover, both from the Land-Use Harmonization 2 (LUH2) database (LUH, 2018; Hurtt et al., 2020).

https://doi.org/10.5194/egusphere-2024-3645
Preprint. Discussion started: 3 January 2025

2 Model, Data and Methods

2.1 Model Description

To simulate TP transport within the riverine system, we employed the Hydrological Discharge (HD) model (Hagemann et al., 2020). The HD model operates on a regular grid with a resolution of 5 minutes (approximately 8-9 km), effectively routing both surface and subsurface lateral water flows from inland areas (sub-grid flow). The model also accounts for water residence times in lakes and wetlands based on their area fractions. River flow is calculated as the transport of water between adjacent grid cells, with the flow direction guided by the terrain morphology. Due to the unique flow directions in the gridded flow network, catchment water budgets are integrated over time at river mouths. The HD model uses sub-daily time steps, with the model output providing daily accumulated river discharge.

The domain setup corresponds to the European region from -1°W to 69°E and 27°N to 72°N, which includes all the catchments for each of the four semi-enclosed European seas (North Sea, Baltic Sea, Black Sea and Mediterranean Sea). The only exception is the Nile catchment, which is not included in the model domain. The flow of the Nile is subject to a strong anthropogenic influence and its dynamics do not correspond to a natural hydrological description (Senay et al., 2014), so it was excluded.

The HD model has been equipped with the capability to transport tracers contained within the water flow following similar calculation to the lateral flow. This model feature has previously been used by Gehlot et al. (2024) to transport dissolved organic carbon. In our case, this capability is used here to estimate TP loads derived from TP concentrations as explained in Section 2.3.

2.1.1 Model Experiments

One first simulation, defined here as hindcast simulation, uses hydrological forcings derived from reanalysis data which is consistent with the atmospheric state and natural variability of the past climate, and P concentrations from the IMAGE-GNM model (Beusen et al., 2015). The historical simulation and three future scenarios use hydrological forcings derived from the global Earth system model GFDL-ESM4 (John et al., 2018) (cf. Sec. 2.2.2), and P concentrations from the new parameterization (cf. Sec. 2.3).

2.2 Data

2.2.1 Total Phosphorus Concentration Observations

For reference values of TP concentration and river discharge, a compendium of river chemistry databases, created as part of the Global Water Chemistry (GLOWACHEM) project at the University of Hamburg, was used. Such a compilation consist of data from monitoring stations from governmental programs Agency (2016); LfU (2017); SEFARI (2020); BfG (2021); Elbe (2021), publications Kempe (1982); van Geldern et al. (2015); Lee et al. (2017); van Geldern et al. (2018); and global river data from GLORICH Hartmann et al. (2014a), GEMStat Programme (2019) and the European Environment Agency EEA (2022).

https://doi.org/10.5194/egusphere-2024-3645
Preprint. Discussion started: 3 January 2025

We removed potential duplicates of sampling locations using a buffer of about 10 meters resolution applied to the coordinates. The data collected have different time lengths, time steps and periods, depending on the data availability at each station. Note that, the associated upstream catchment area is not provided. Hence, the distance to the coast was used as a suitability measure when the proximity to the shoreline was necessary.

TP loads were calculated using observed discharge time series from the same stations at the same sampling intervals as the TP concentrations. In cases where sampled discharge values were not available, averaged discharge from the station was used (if available). For the station at Geesthacht on the Elbe river, the discharge time series specific to the Elbe catchment from E-Hype model (Donnelly et al., 2015) was used.

The datasets provide instantaneous measurements, predominantly at a monthly frequency, which restricts our analysis to monthly averaged values despite the daily frequency of the model output. Missing values are commonly found within the observational datasets; however, in order to maximize data usability, when gaps of consecutive missing values did not exceed 12 months, they were interpolated linearly over time. For the climate analysis, a robust climatology was required, in this case only stations with time series of more than 5 consecutive years were included.

2.2.2 Forcings

2.2.3 Future Development Scenarios

Land use developments from the Socioeconomical Shared Pathways (SSP) scenarios combined with specific Representative Concentration Pathways (RPC) scenarios and the respective hydrological simulations were used to perform our TP load projections. The SSP scenarios represent narratives describing different developments of the society, while the RCP scenarios depict climate change projections based on different greenhouse gas (GHG) emission pathways and defined by radiative forcing values by the year 2100. The scenarios utilized in this study are described as follows (O'Neill et al., 2017; Riahi et al., 2017; van Vuuren et al., 2011, 2017):

SSP1-RCP2.6: A sustainable and green scenario that assumes global cooperation to preserve natural resources and low energy usage, thereby focussing on human well-being rather than economical growth. It aims at a radiative forcing of 2.6 W/m^2 by the year 2100 to limit global mean temperature increase to 2°C.

SSP3-RCP7.0: A regional rivalry scenario that assumes regional conflicts that push countries to focus on domestic issues. It prioritizes national and regional security with energy and food as primary issues at the expense of broader-based development. It implies that some regions would suffer from drastic environmental damage. In regard of radiative forcings, it is a upper-middle scenario with 7 W/m^2 by the year 2100.

SSP5-RCP8.5: A fossil-fueled development scenario that leads to social and economic growth at the cost of exploitation of fossil fuel and coal resources. Strong technological progress is expected to solve local environmental problems. Event tough considered implausible by now (Ritchie and Dowlatabadi, 2017), this scenario with a radiative forcing of 8.5 W/m^2 by the year 2100 is an interesting extreme case that we investigated to test the boundaries of our methodology.

https://doi.org/10.5194/egusphere-2024-3645
Preprint. Discussion started: 3 January 2025

2.2.4 Hydrology Simulations Approach

Following similar setup as in Hagemann and Stacke (2023), daily surface and subsurface runoff (drainage) were generated with the global hydrology model HydroPy (Stacke and Hagemann, 2021) to be used as input fields for the HD model simulations.

For the hindcast simulation, HydroPy was forced with the Global Soil Wetness Project Phase 3 (GSWP3) (Dirmeyer et al., 2006; Kim, 2017) atmospheric dataset. Kim (2017) derived the GSWP3 dataset from the 20th century reanalysis (Compo et al., 2011) and applied observation-based bias correction procedures at the 0.5° resolution of the GSWP3 product that covers the years 1901-2014. As in our study, we focus on the years 1979-2014; the years 1901-1978 were considered as spin-up period.

For the historical (Stacke and Hagemann, 2021) and the three scenario simulations, we used forcing data (Lange and Büchner, 2021) based on the Coupled Model Intercomparison Project Phase 6 (Eyring et al., 2016) output of the Earth system model GFDL-ESM4 (John et al., 2018), which were downscaled to 0.5° and bias-corrected as part of the Inter-Sectoral Impact Model Intercomparison Project (ISIMIP) (Warszawski et al., 2013).

2.2.5 Simulated Total Phosphorus Concentrations

TP concentrations were obtained from two distinct datasets, depending on the type of simulation. For the hindcast simulation, TP concentrations were derived from the Integrated Model to Assess the Global Environment-Global Nutrient Model (IMAGE-GNM) socio-economic model (Beusen et al., 2015). IMAGE-GNM simulates the global environmental impacts of human activities and is frequently employed to develop scenarios that support environmental assessments and provide insights into the potential consequences of various response strategies (Beusen et al., 2015, 2016). It has an annual frequency output with a spatial resolution of 0.5°, and provides load values for all TP aggregates: agricultural and natural land, weathering, allochthonous organic matter input to rivers, aquaculture and wastewater.

To estimate TP loads under future scenarios influenced by human activities, data from the Land-Use Harmonization 2 (LUH2) project were utilized (LUH, 2018; Hurtt et al., 2020). These scenarios correspond to different climate policy narratives from the Socioeconomic Shared Pathways. The LUH2 dataset provides fertilizer application data in the form of nitrogen (N) amounts only. Consequently, a conversion to P was required, the methodology for which is described in detail in in the section 2.3.4.

2.3 Methods

TP concentrations for the hindcast simulation were obtained from each of the aggregate P loads from the IMAGE-GNM model (Beusen et al., 2016) by calculating the ratio of P load to total runoff from the HydroPy model in the common period that overlaps between the HydroPy hindcast and IMAGE-GNM data, i.e. from 1979 to 2000. Original P loads in Beusen et al. (2016) were simulated using total runoff from the PCR-GLOBWB hydrological model forced by ERA40 reanalysis data. To verify that no bias was introduced by the use of different hydrological datasets, we compared the inferred concentration from the weathering aggregate with the concentration calculated directly using the weathering parameterization by Hartmann et al. (2014b). Both magnitudes were consistent.

https://doi.org/10.5194/egusphere-2024-3645
Preprint. Discussion started: 3 January 2025

As for the scenario simulations, only inferred concentrations from aquaculture and allochthonous organic matter from IMAGE-GNM were used. Concentrations from wastewater, natural land, and pasture areas were remapped into urban, forest and pasture areas using the corresponding land use types from LUH2 dataset. This transformation assigns concentrations to each of the LUH2 land types, ensuring that values remain conservative at the catchment scale for the years with the common period. Concentrations for weathering, atmospheric deposition and cropland were calculated as follows:

2.3.1 Process parameterizations

2.3.2 Weathering

To account for background phosphorus concentrations from weathering, the parameterization by Hartmann et al. (2014b) was implemented in the HD model. This scheme calculates the chemical weathering flux (F_{CW}) based on lithology classes, temperature, soil shielding, and runoff, and it is expressed as:

$$F_{CW(x,y,t)} = \sum_{j}^{m-types} b_j(T)_{(x,y,t)} \cdot q_{(x,y,t)} \quad (1)$$

where $b_j(T)$ is a factor for each of the lithological classes m and it is dependent of the near-surface temperature T. Total runoff is denoted by q. Subindices x, y and t indicate the two dimensional spatial and temporal dependency of the variables, respectively. The lithological dataset was obtained from Hartmann and Moosdorf (2011).

2.3.3 Atmospheric Deposition

The estimation of direct atmospheric deposition inputs is based on the water surface area of the catchment from water bodies and streams. Over land areas the net balance is considered zero. Behrendt et al. (2003) estimated a global geometric mean of 0.0037 [g P m-2 yr-1] under the assumption that, in average, the water surface constitutes approximately around 1 percent of the total area. Tipping et al. (2014) account for a value of 0.027 g P m-2 yr-1. In a more recent study, Berthold et al. (2019) updated the estimate of phosphate deposition over water areas to 16.7 [kg km-2 y-1] that is equivalent to a phosphorus load of 0.0074 [g m-2 yr-1]. The latest estimate is used in our simulations.

2.3.4 Fertilizer Application

Long-term application of fertilizers in agricultural areas significantly contribute to water pollution in rivers. P losses from crop and pasture areas due to leaching and runoff processes are already one of the aggregates of the total phosphorus in the Beusen et al. (2016) dataset. After computing the concentrations as previously described, they were directly applied as forcings in the hindcast simulation. However, for the future climate simulations, such concentrations are not available. To overcome the lack of data, we inferred the P losses from the nitrogen (N) application information from the Land-Use Harmonization 2 dataset (LUH2) (LUH, 2018; Hurtt et al., 2020), which includes fertilizer application information in different land-use scenarios and

https://doi.org/10.5194/egusphere-2024-3645
Preprint. Discussion started: 3 January 2025

socio-economical pathways for future projections. The phosphorus application P^i_{fert}, applied to different crop and pasture area types i is calculated as follows:

$$P^i_{fert(x,y,t)} = N^i_{fert(x,y,t)} \cdot r_{N:P2O5} \cdot k_{P2O5:P} \tag{2}$$

where N^i_{fert} [kg N ha-1] is the amount of nitrogen application from the LUH2 dataset, $r_{N:P2O5}$ corresponds to nitrogen-phosphate ratio (N:P2O5) in the fertilizer. The N:P2O5 ratio is subject to change based on the type of fertilizer applied, the current country policies, etc. (Comission, 2019; Motesharezadeh et al., 2017). In this case, we take the ratio of 130:39.3 (Hua and Zhu, 2020). The conversion factor from phosphate to elemental phosphorus, $k_{P2O5:P}$, is based on the atomic weight of phosphorus and oxygen of 30.97 and 15.99 g/mol, respectively, and becomes 61.94/141.88, i.e. 0.44. The subindices x, y and t indicate the two dimensional spatial and temporal dependency of the variables, respectively.

The phosphorus concentration losses P^i_{conc} are then computed as:

$$P^i_{conc(x,y,t)} = P^i_{fert(x,y,t)} \cdot f_{Ploss} \cdot S \cdot f^i_{lc(x,y,t)} \tag{3}$$

Here, f_{Ploss} represents the fraction of P applied to the croplands that is lost through runoff and leaching processes. This value has been widely discussed because of its large uncertainty, which results from the different conditions under which fertilizers are applied to different agro-ecosystem configurations (e.g. plant and soil types, cropland physiology, application timing, weather conditions, etc.). It could range from as low as 0.03% to approx. 7%, and in exceptional cases up to 30% (Hart et al., 2004; Lun et al., 2018; Hua and Zhu, 2020). Therefore, in this parameterization, this value is treated as a tuning factor, and an optimal value of 3.5% was chosen. S [m-1] is the inverse of the soil depth. The soil depth is a sensible factor in the parameterization as well. Olarewaju et al. (2009) report that higher concentrations of P are located in the near-surface soil depth of 0-15 cm compared to deeper layers up to 75 cm. They demonstrated a positive correlation for phosphorus content between the 0-15 cm soil depth and the P concentration in rivers adjacent to agricultural fields (cf. Table 3 in Olarewaju et al. (2009)). Other studies typically sample from a soil depth of 20 cm (Ekholm et al., 2005). Hence, in this parameterization, a soil depth of 0.2 meters was adopted. f^i_{lc} is the land cover fraction for each of the cropland types i from LUH2.

Phosphorus load $P^{cropland}_{load}$ is calculated by integrating P concentrations across all cropland types and then multiplied by the total runoff q:

$$P^{cropland}_{load(x,y,t)} = \sum_{i}^{n-types} (P^i_{conc(x,y,t)}) \cdot q_{x,y,t} \tag{4}$$

https://doi.org/10.5194/egusphere-2024-3645
Preprint. Discussion started: 3 January 2025

2.3.5 Metrics

2.3.6 Seasonality

Two metrics have been applied to the observed and simulated data at the station locations to determine seasonality. The first consists in applying a lagged autocorrelation to the detrended monthly time series, similar to the method proposed in Wang et al. (2006) for an arbitrary periodicity, but in our case we assume a fixed 12-months frequency, corresponding to an annual seasonality signal. The result obtained from the autocorrelation function is then analyzed by searching for a peak in the 12th month with an autocorrelation higher than 0.5 and whose difference from the preceding trough is at least 0.1. If such peak is not found no periodicity is assumed.

The second metric consists on the calculation of the Seasonal Strength index according to Hyndman and Athanasopoulos (2018). This metric is based on the additive decomposition of the time series and it takes the form:

$$F = max\left(0, 1 - \frac{var(R_t)}{var(S_t + R_t)}\right) \tag{5}$$

where S_t and R_t are the seasonal and residuals components of the time series, with t denoting the temporal dimension. By construction the value of the index varies between 0 and 1, and indicates weak and strong seasonality, respectively.

2.3.7 Kling-Gupta Efficiency index

The Kling-Gupta Efficiency (KGE) index (Gupta et al., 2009; Kling et al., 2012) is commonly used to evaluate the performance of hydrology models. The KGE index calculates a score between simulated and observed time series by considering their correlation, variability and averaged bias:

$$KGE = 1 - \sqrt{\sum_{i=1}^{3} (\alpha_i - 1)^2} \tag{6}$$

where α_1 equals the Pearson correlation coefficient, $\alpha_2 = \frac{CV_{sim}}{CV_{obs}}$ is the coefficient of variation ratio for simulated and observed time series with $CV_j = \frac{\sigma_j}{\mu_j}$, where σ_j and μ_j are the standard deviation and mean value, respectively. $\alpha_3 = \frac{\mu_{sim}}{\mu_{obs}}$ is the mean value ratio. As noted in Knoben et al. (2019), considering the case the simulated time series equals a constant value equivalent to the average of the observed time series, the KGE becomes -0.41. Time series data with KGE scores between -0.4 and 1 are a better solution than applying a constant observed value over time, we consider that scores within this range indicate a 'good' model performance.

https://doi.org/10.5194/egusphere-2024-3645
Preprint. Discussion started: 3 January 2025

3 Results and Discussion

3.1 Seasonality Determination

The majority of fertilizer applications follow seasonal practices derived by selecting months when the best environmental conditions are more favourable for plant growth. To investigate whether these practices generate a detectable signal in TP concentrations in the river flow at catchment scale, i.e. near the river mouth at the coast, two seasonality tests, monthly correlation and Seasonality Strength Index (SSI), were applied to data from measurement stations. Due to the limited availability of monitoring stations located at river mouths, a filtering criterion based on the proximity of stations to the nearest coastline was applied, with a maximum allowed distance of 100 km. Out of a combined total of 5,961 monitoring stations globally, from both GEMStat and GLORICH databases, 360 stations (96 from GEMStat and 264 from GLORICH) met into this criterion.

To assume seasonality, the arbitrary threshold value of 0.6 was used for both methods. After applying the seasonality test to the selected stations sample, median values from the correlation method and SSI were 0.07 and 0.09, respectively. Only one station, at USA, was found to have an SSI value of 0.67. The Danube had a correlation of 0.6 and its SSI was 0.23. For the Elbe, respective values are 0.30 and 0.04. Although P losses from agricultural practices increase TP concentrations in river discharge, the result suggests that the effects of seasonality are likely to be dispersed over time, possibly due to catchment hydrology dynamics yet to be studied.

While dissolved and particulate forms of TP were not the focus of this study, it is well-established that such forms exhibit clearly seasonal variability, particularly in river estuary regions where biogeochemical productivity is higher due to the slower flow rate of the river hydrodynamic (Iglesias et al., 2024). However, measurements from selected monitoring stations reveal that there is an absence of discernible seasonal patterns. Hence, the seasonality signal in our parameterization of TP losses was neglected (Sec. 2.3.4).

3.2 Model Performance

To evaluate the quality of the simulated TP loads by the HD model, time series from coastal and in-land measurement stations from GEMStat and GLORICH databases were compared to model results extracted from the model grid at respective station locations. This comparison consists on applying the KGE to observed and hindcast simulation data within the European region corresponding to the model domain. To ensure that observed data comply with a minimum climatology, stations with at least 5 years of continuous recorded data were selected.

By design, KGE index values below of -0.41 mark a threshold where the model performance becomes worse than simply using the mean of the observed data as a predictor (Knoben et al., 2019). Results for TP loads from the hindcast simulation (driven with forcings from the reanalysis dataset and TP concentrations from IMAGE-GNM) generally exceed this -0.4 threshold (left panel in Fig. 1). However, TP load is the result from the combined signal of TP concentration and discharge values. The KGE index for discharge values (right panel of the same figure) shows that for most stations, the degradation of TP load signal is primarily driven by TP concentrations rather than the discharge. Nonetheless, few stations still exhibit low KGE values in combination of stations with good performance within the same river system. Various factors could contribute to this

https://doi.org/10.5194/egusphere-2024-3645
Preprint. Discussion started: 3 January 2025

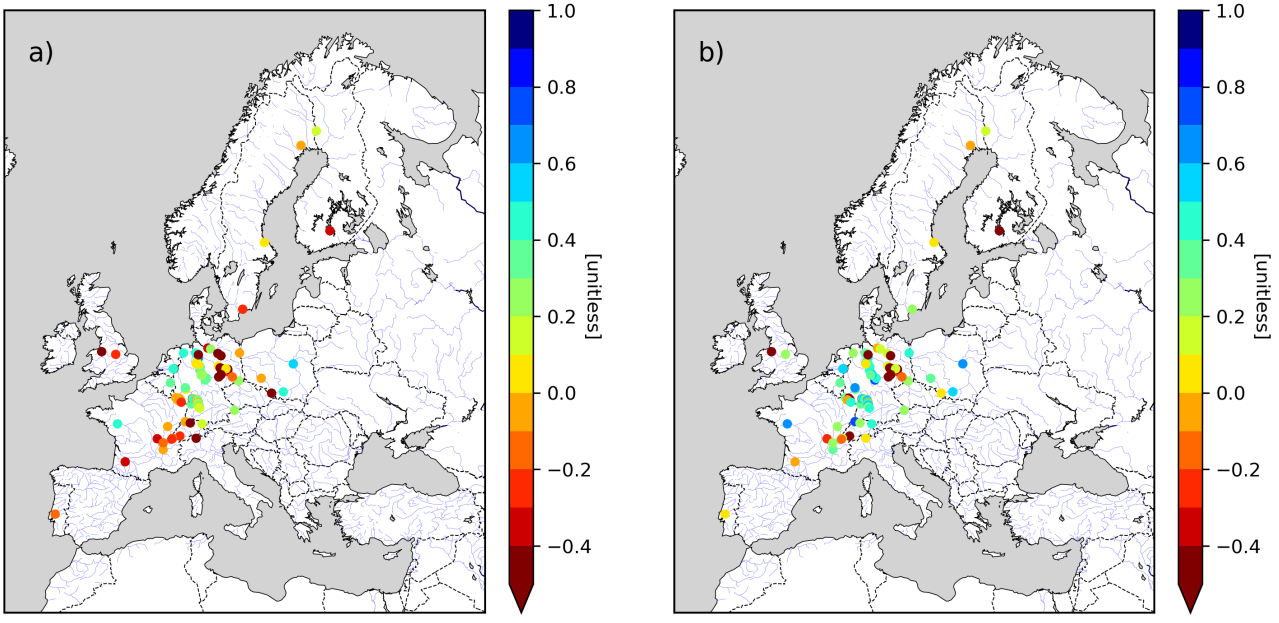

Figure 1. KGE index for TP load (a) and discharge (b) for the hindcast simulation.

bias. A plausible explanation is that these stations are located at tributaries to the main river branch rather than along the main stream. In such cases, subgrid-scale hydrological processes, which are not captured by the model, may account for the varying performance across the same river system.

The comparison of the hindcast and the historical simulation is done using two of the KGE components, CV and mean ratios, for TP concentrations and discharge (Fig. 2). The ideal value of such ratios is 1, i.e. the simulated variability and mean values of each simulation would be in perfect agreement with the corresponding observed values. Fig. 2 shows that in general both simulations have similar bias; for stations where the hindcast simulation underestimates (overestimates) the observations, the historical simulation shows similar behaviour. However, for the mean concentration ratios (Fig. 2b), the difference in the bias is explained by the horizontal redistribution of the concentrations in the historical simulation. This redistribution does not indicate a degradation or improvement in the concentrations.

3.2.1 Catchment Scale

The model validation at a catchment scale is limited to a few number of catchments due to the scarcity of available observations. To ensure that the station is representative of the catchment dynamics, and therefore comparable with the model output, the ratio of the distance from the station to the coastline relative to the catchment area was calculated. Only catchments with ratios less than 0.01 m^{-1} were considered.

Figure 3 shows a comparison of normalized simulated TP load and discharge with station data. Observational data for each catchment correspond to a station in the corresponding river which location was not farther than 120 km from the coast within

https://doi.org/10.5194/egusphere-2024-3645
Preprint. Discussion started: 3 January 2025

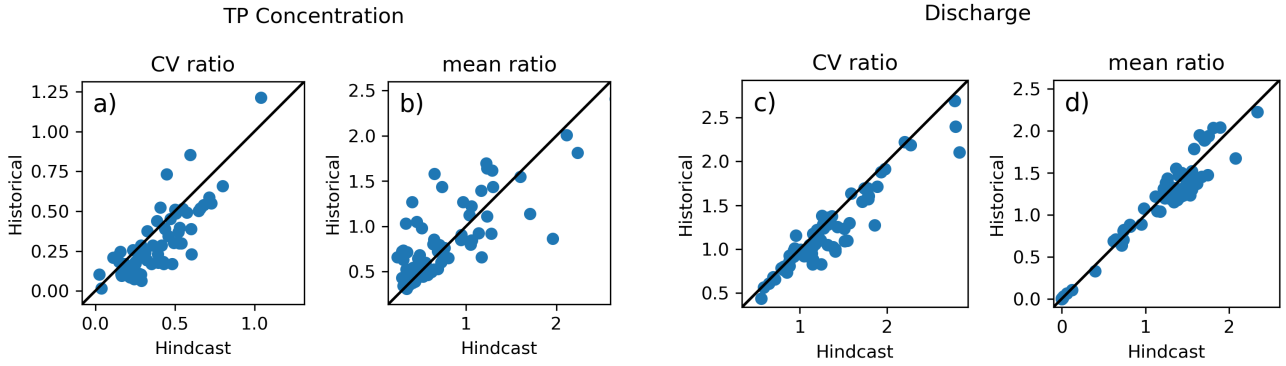

Figure 2. Comparison of two of the KGE components, coefficient of variation (a and c) and mean value (b and d) ratios, for TP concentrations and discharge between hindcast and historical simulations.

the European region (in contrast to the previous seasonality analysis that uses 100 km and considers stations globally). The boxes represent the 1st and 3rd quartiles and the median of each dataset. The whiskers show the 5th and 95th percentiles. Values outside the whiskers limits are represented by dots. The comparison is restricted to a common time period between the observations and model runs, therefore each catchment might have different time length but only those stations with a time series longer than 5 years were selected.

The discharge is slightly overestimated at the upper end of the observed variability, but low and median values are well represented in the simulation. In contrast, the simulation tends to underestimate TP loads derived by low TP concentrations. This discrepancy is notably pronounced in the three largest catchments analyzed (Vistula, Elbe, and Oder catchments). Yet, as only a very limited number of measurement stations meet the catchment-criteria, it is not possible to draw definitive conclusions regarding the model performance at catchment level.

3.2.2 Basin Scale

TP load budgets have been calculated for the four semi-enclosed European seas. Table 1 shows annual TP loads contribution for each catchment to its respective basin in the historical simulation within the period from 1979 to 2014. The area of the catchment is not correlated with TP load contributions, which suggest that sources from land use and wastewater are more relevant to the catchment budget. We define the Small Contributions Integral (SCI) as the integration of individual contributions of less than 1.5% of the total basin load. Most of such contributions might originate from relatively small rivers, typically as a result of complex orography with little or no human influence. Consequently, the primary P sources are predominantly from natural lands. These contributions are frequently underrepresented in observational networks. Although such individual contributions are small, the SCI results in 25 to 60% of the basin total (Table 1).

https://doi.org/10.5194/egusphere-2024-3645
Preprint. Discussion started: 3 January 2025

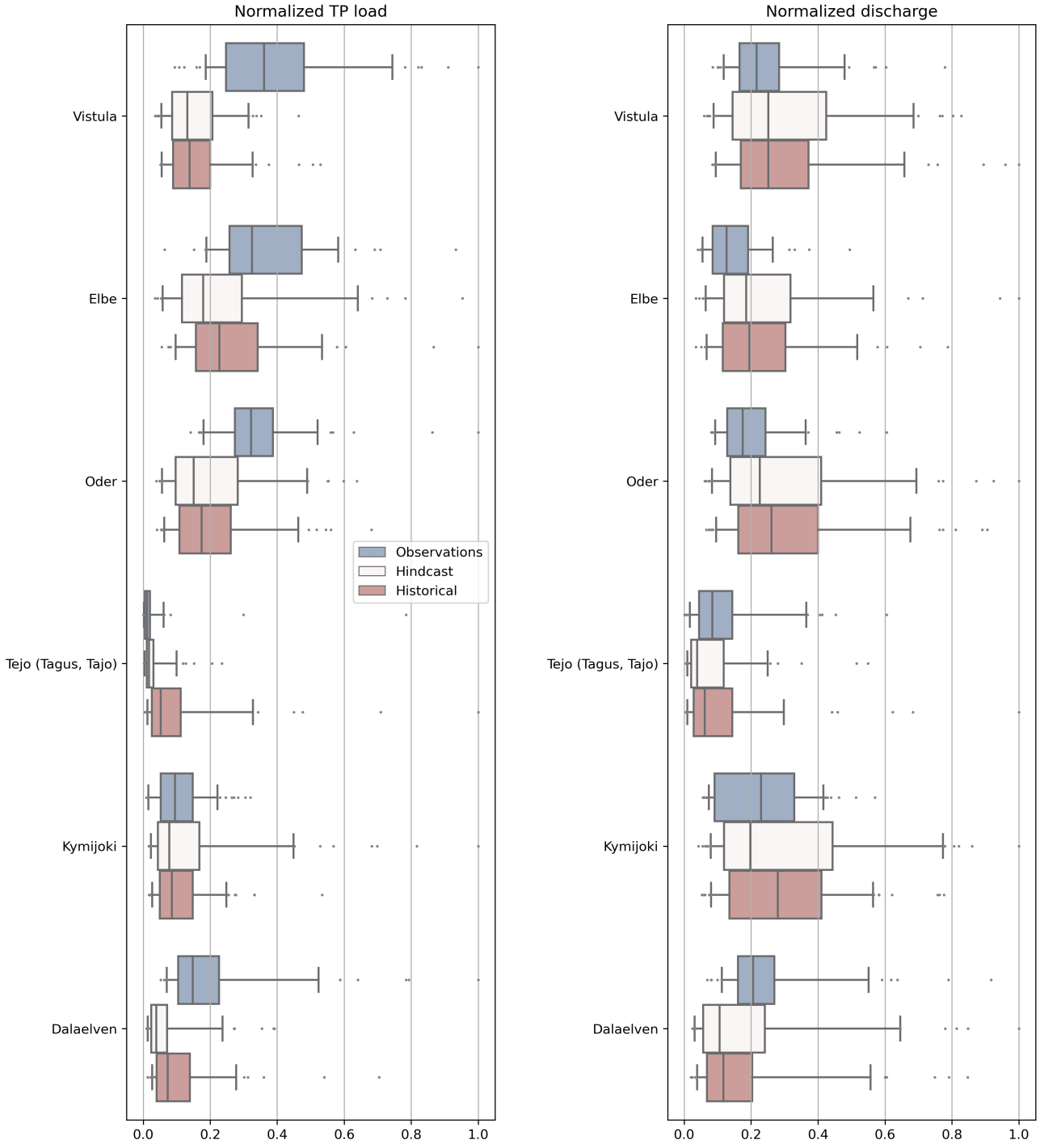

Figure 3. Comparison of normalized TP load (left) and discharge (right) between observed data and model simulations.

https://doi.org/10.5194/egusphere-2024-3645
Preprint. Discussion started: 3 January 2025

Historical trends have been calculated following a similar approach to Behrendt et al. (2003). To assess the effectiveness of nutrient pollution reduction strategies implemented collaboratively by several Northern European countries, such as those outlined in the International Conference on the Protection of the North Sea (ICN) and the Helsinki Commision (HELCOM) (ICN, 1987), and later in the Baltic Sea Action Plan (BSAP) (HELCOM, 2007), Behrendt et al. (2003) calculated TP loads averages along different periods at basin level for the Baltic, North and Black seas, but also for the largest German rivers (Elbe, Rhine and Weser). Table 2 presents such averages from the GIS-based model Modelling Nutrient Emissions in River Systems (MONERIS) (Behrendt et al., 2003) and from the HD model hindcast and historical simulations. For reference values, observations for the Elbe river from the GLOWACHEM dataset and HELCOM data (Gustafsson et al., 2012; Svendsen and Gustafsson, 2023) for the Baltic Sea basin were used. For the Elbe river, both models compare well in magnitude and trend from observations. Similar results were obtained for the Weser river. However, for the rest of the basins, both models diverge significantly, showing discrepancies of up to one order of magnitude. For the Baltic Sea, both models underestimate TP load values compared to HELCOM data, in particular the MONERIS model. Nevertheless, it is worth noting that, due to the lack of nutrient observations, TP load estimates from HELCOM have a significantly large uncertainty, ranging from 20 to 50% (Svendsen and Gustafsson, 2023). The bias is attributed to TP concentrations values only. The averaged discharge value from the HD model of 15,829 m^3/s is within the range of reported values of 15,602 m^3/s and approx. 17,000 m^3/s (Svendsen and Gustafsson, 2023; Raudsepp et al., 2023).

https://doi.org/10.5194/egusphere-2024-3645
Preprint. Discussion started: 3 January 2025

Table 1. Averaged catchment contributions and basin totals for TP load for each of the four European basins within the period 1979-2014. TP load is presented in metric kilotons per year [kt y-1] as well as a percentage relative to the basin total budget. Rivers which individually contribute with less than 1.5% are all integrated under the Small Contributions Integral (SCI).

(a) North Sea

Catchment	TP load	Percent.
SCI	16.1	25.6
Trent	7.0	11.1
Rhine	6.8	10.9
Themse	6.3	9.9
Elbe	5.6	9.0
Scheldt (Schelde)	5.3	8.4
Meuse	4.3	6.8
Weser	3.7	5.8
Ijssel	2.3	3.7
Great Ouse	1.6	2.5
Ems	1.5	2.4
Somme	1.3	2.1
Tay	1.3	2.0
TOTAL	63.1	100.0

(b) Baltic Sea

Catchment	TP load	Percent.
SCI	12.1	45.7
Oder	3.2	11.9
Vistula	3.1	11.6
Newa	1.6	6.1
Neman	1.4	5.3
Maelaren/Norrström	1.0	3.8
Narva	0.9	3.3
Daugava	0.8	3.0
Goeta Vaenern	0.7	2.8
Pregolya (Pregel)	0.6	2.4
Kiskonjoki	0.6	2.3
Lielupe	0.5	1.8
TOTAL	26.5	100.0

(c) Black Sea

Catchment	TP load	Percent.
SCI	21.2	29.5
Danube	7.2	10.0
Kizilirmak	5.9	8.2
Don	5.6	7.7
Sakarya	5.0	7.0
Rioni	3.9	5.4
Dnjepr	3.2	4.4
Kuban	2.7	3.7
Dniestr	2.4	3.4
Yesilirmak (Kelkit)	2.3	3.2
Southern Bug	1.8	2.6
Coruh	1.7	2.3
Enguri	1.4	2.0
Mius	1.1	1.6
Kalmius	1.1	1.6
TOTAL	71.8	100.0

(d) Mediterranean Sea

Catchment	TP load	Percent
SCI	300.0	60.4
Ebro	40.5	8.2
Orontes (Asi)	29.5	5.9
Medjerda	26.3	5.3
Jucar	18.3	3.7
Moulouya	17.6	3.5
Jebel Akhdar	14.1	2.8
Po	13.6	2.7
Chelif	10.5	2.1
Rhone	10.0	2.0
Ceyhan	8.8	1.8
Segura	7.5	1.5
TOTAL	496.7	100.0

https://doi.org/10.5194/egusphere-2024-3645
Preprint. Discussion started: 3 January 2025

Table 2. Averages of TP loads (in kilotons per year $[kt/y]$ for different historical periods and datasets. Observed data includes GLOWACHEM and HELCOM, while simulated data comprises MONERIS and HD model

Catchment	1983-1987	1993-1997	1998-2000	2001-2014
Elbe				
GLOWACHEM	9.5	5.4	4.4	2.9
MONERIS	8.3	4.7	3.5	-
HDmodel (Control)	6.0	4.3	3.9	-
HDmodel (Historical)	7.7	5.3	5.3	4.3
Rhine				
MONERIS	29.1	11.9	10.8	-
HDmodel (Control)	11.6	7.7	7.2	-
HDmodel (Historical)	9.1	6.7	5.9	5.1
Weser				
MONERIS	4.9	2.2	2.2	-
HDmodel (Control)	3.9	2.6	2.3	-
HDmodel (Historical)	4.8	3.4	3.0	2.9
North Sea				
MONERIS	77.2	29.8	27.1	-
HDmodel (Control)	70.8	54.8	59.8	-
HDmodel (Historical)	75.4	62.3	57.7	54.4
Baltic Sea				
MONERIS	4.1	1.6	1.4	-
HELCOM	60.2	42.6	43.0	31.6
HDmodel (Control)	28.0	25.1	27.7	-
HDmodel (Historical)	34.1	25.9	23.8	23.1
Black Sea				
MONERIS	10.5	5.0	4.7	-
HDmodel (Control)	62.0	72.4	79.3	-
HDmodel (Historical)	69.6	79.2	71.1	70.6
Mediterranean Sea				
HDmodel (Control)	378.4	379.3	358.4	-
HDmodel (Historical)	398.0	525.7	526.5	513.5

315 Several factors could account for the discrepancies between the models. One potential source of difference is the representation of small catchments; for instance, MONERIS may inaccurately represent catchments smaller than 50 km^2 due to the lack of availability of high-resolution maps (Behrendt et al., 2003). Additionally, variations in the datasets used to derive P concentrations, as well as differences in the spatial distribution schemes applied in each model, may contribute to these incon-

https://doi.org/10.5194/egusphere-2024-3645
Preprint. Discussion started: 3 January 2025

sistencies. A more detailed analysis is necessary to accurately attribute the underlying causes of the discrepancies, which is beyond the scope of the present study.

According with the ICN, nutrient pollution reduction policies aimed to achieve a 50% reduction in TP emissions by the last decade of the 20th century compared to levels from the late 1980s. While this trend is well captured by the MONERIS model for the northern European basins, TP concentrations in the HD model do not exhibit a similarly pronounced negative trend. Southern European basins have not been subject of such policies, and therefore the trends tend to increase from the 80s and stabilize in the consecutive periods.

To the best of our knowledge, there are no existing reports providing estimates (observed or simulated) of TP loads for the Mediterranean Sea. According to our calculations, the TP budget for the basin is about 500 kt/y, with up to 60% of the load coming from the SCI alone.

3.3 Response to Climate and Socioeconomic Scenarios

Long-term TP losses projections have been simulated to assess the P contribution from eutrophication and climate change in the European semi-enclosed seas based on three projected narratives (Sec. 2.2.3). Figures 4 and 5 show the progression of nutrient pollution, and Table 3 provides a quantification of the projected changes by the end of the century (2081-2100) with respect to the baseline period (1991-2010).

https://doi.org/10.5194/egusphere-2024-3645
Preprint. Discussion started: 3 January 2025

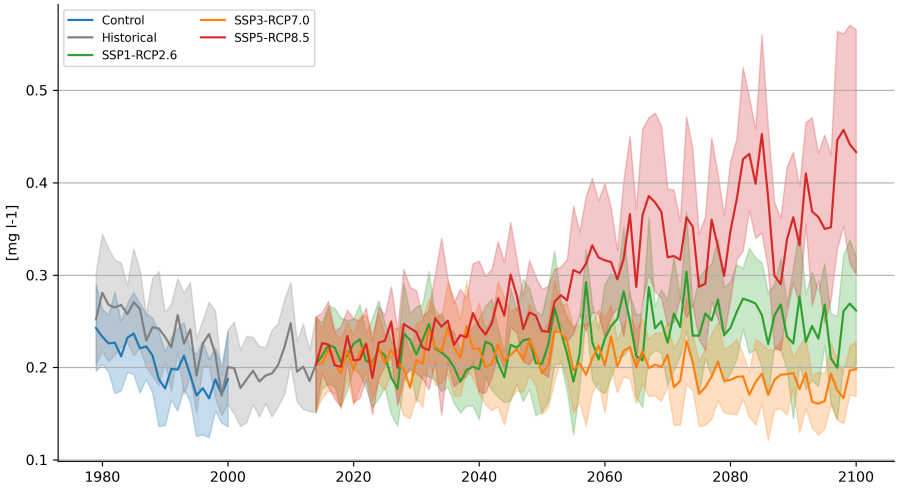

(a) North Sea

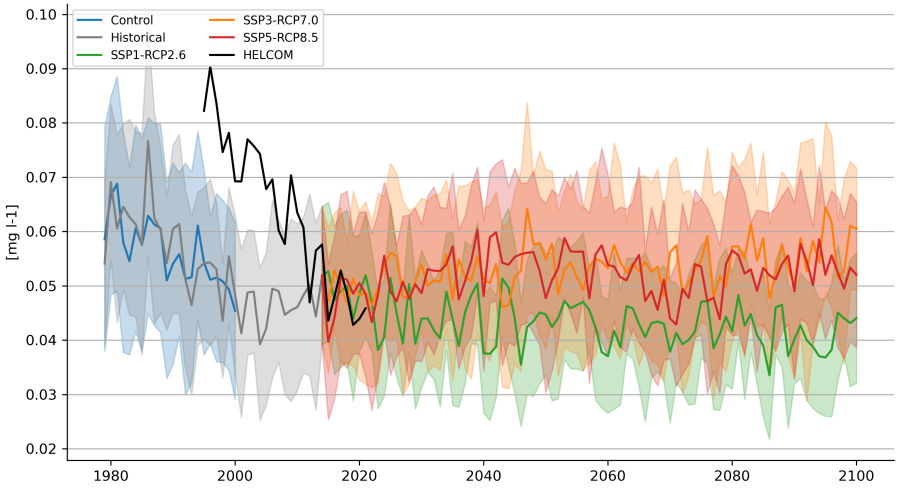

(b) Baltic Sea

Figure 4. Total phosphorus concentration scenarios (in milligrams per litre $[mg/l]$) for the North and Baltic seas. Solid lines represent yearly averages and shaded areas the yearly variability as one standard deviation. Observational data from HELCOM (in black) has been included in the case of the Baltic Sea.

https://doi.org/10.5194/egusphere-2024-3645
Preprint. Discussion started: 3 January 2025

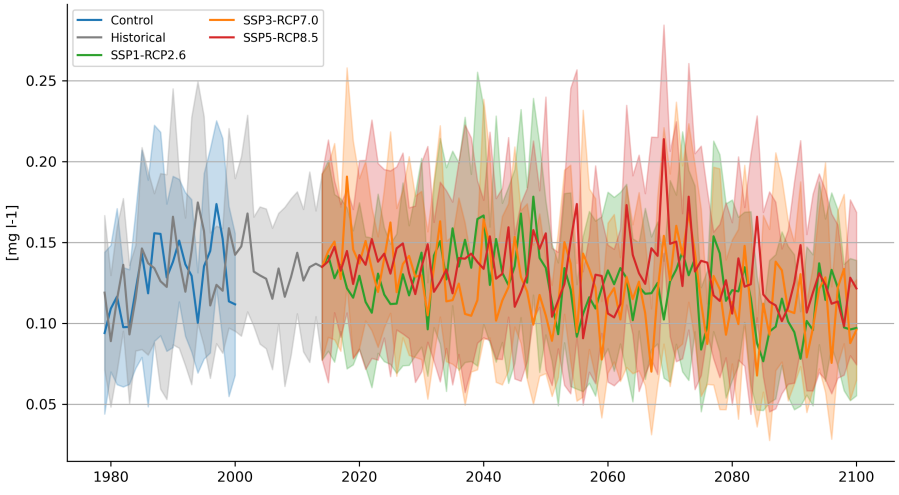

(a) Black Sea

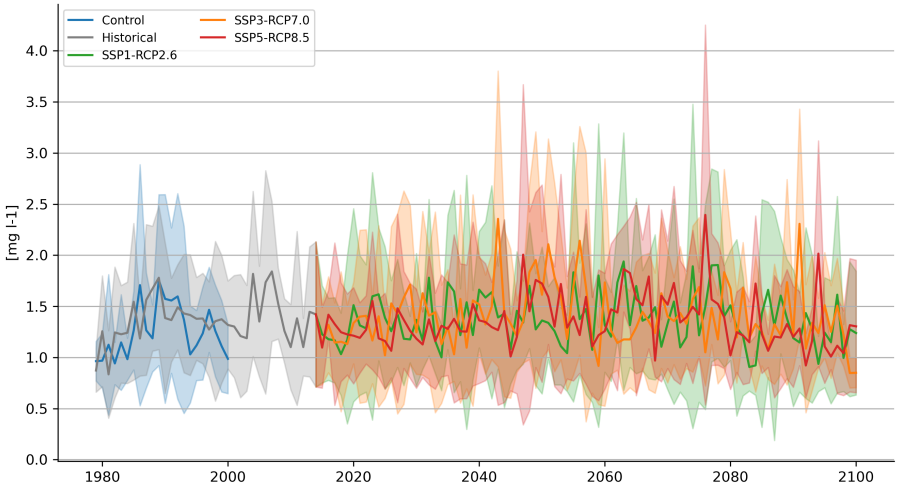

(b) Mediterranean Sea

Figure 5. Same as Fig. 4, but for the Baltic and Mediterranean Seas.

https://doi.org/10.5194/egusphere-2024-3645
Preprint. Discussion started: 3 January 2025

Table 3. Estimated changes for discharge, TP concentrations and TP loads (in percentage) by the end of the century (2081-2100) with respect to the baseline period (1991-2010). Baseline period averages are provided for each variable with their respective units. Positive (negative) percentages indicate an increase (reduction) in comparison to the corresponding baseline averaged value.

Scenario	**North Sea**	**Baltic Sea**	**Black Sea**	**Med. Sea**
Discharge $[m^3/s]$	**8661**	**15785**	**16897**	**10419**
SSP1-RCP2.6	10.4	4.8	3.6	-2.2
SSP3-RCP7.0	6.5	17.9	-4.8	-24.8
SSP5-RCP8.5	2.9	13.1	-8.7	-28.3
TP conc. $[mg/l]$	**0.2**	**0.05**	**0.1**	**1.4**
SSP1-RCP2.6	11.1	-22.2	-21.5	-9.4
SSP3-RCP7.0	-18.6	5.5	-18.5	-5.2
SSP5-RCP8.5	71.4	-0.5	-9.2	-10.7
TP loads $[kt/y]$	**63.2**	**26.4**	**72.7**	**502.4**
SSP1-RCP2.6	22.8	-16.9	-17.1	-8.6
SSP3-RCP7.0	-12.7	29.7	-19.2	-30.0
SSP5-RCP8.5	75.6	17.4	-13.5	-37.3

Regional trends are significantly influenced by key factors from the SSP narratives (including policies, population growth, and land-use changes, etc), as well as climate change signals related to temperature and precipitation variations across sub-regions.

For the Southern European Seas, i.e. the Black and Mediterranean Seas, our projections indicate a reduction in TP loads ranging from 17 to 20% for the Black Sea and from 9 to 37% for the Mediterranean Sea (Table 3). This reduction is a consequence of two factors: firstly, a projected decrease in precipitation in southern Europe (Kjellström et al., 2011; Kovats et al., 2014), which reduces river discharged values. Secondly, water scarcity and compound heat and dry conditions diminish population growth and crop production (Calvin et al., 2023), leading to a reduction of sub-basin budgets for TP concentrations. River discharge and TP concentrations signals compensate each other, resulting in low variability in TP loads between scenarios for the Black Sea, where as for the Mediterranean Sea, the variability between scenarios for TP loads is dominated by the reduction in river discharge.

Whereas for the Northern Seas, there is a distinguishable influence of policies and human activities (Fig. 4). For the Baltic Sea, in the historical period, TP loads from the model output are approximately 30% lower than those reported in the HELCOM database. However, given the 20-50% uncertainty range in HELCOM data (Svendsen and Gustafsson, 2023), the model's results remain within the margin of uncertainty. The negative trends in the historical period for the Baltic and North Seas are consistent with agricultural water pollution reduction policies established in the 1980s. For the projections, precipitation is likely to increase in northern Europe for all three scenarios (Kjellström et al., 2011; Kovats et al., 2014) (Table 3), which

https://doi.org/10.5194/egusphere-2024-3645
Preprint. Discussion started: 3 January 2025

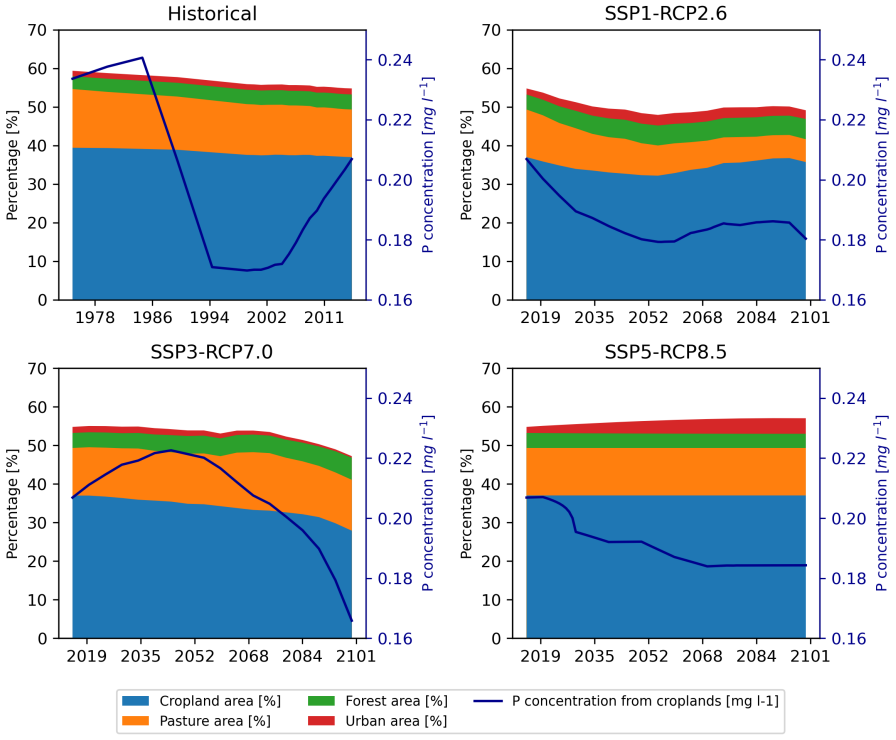

Figure 6. Land-use evolution (in percentage) for the Elbe catchment for different SSP narratives. The solid line represents the catchment average of surplus P concentration (in mg l-1) from croplands that serves as forcings for the HD model.

drives the larger TP load values for the SSP3-RCP7.0 and SSP5-RCP8.5 scenarios despite small changes in concentrations. In SSP1-RCP2.6, the strong reduction of approximately 22% in TP concentrations, leads to a decrease of abount 17% in TP load.

For the North Sea, both SSP1-RCP2.6 and SSP5-RCP8.5 scenarios show positive trends at the end of the century, particularly in the former scenario. To better understand the trends of each scenario, land-use changes and surplus P concentration forcings for each narrative have been plotted for the Elbe catchment only which well represents the regional trends (Fig. 6). For the Elbe and North Sea region, SSP1-RCP2.6 and SSP5-RCP8.5 depict a rapid economic growth that drives social development and a demand of agricultural products Mitter et al. (2020). Despite that surplus P concentrations are reduced, either by technological advances or future pollution policies (Mitter et al., 2020), social development progresses and population grows (KC and Lutz, 2017; Stehfest et al., 2019), leading to a larger demand of food, and an expansion of agricultural and urban areas. Fig. 4 shows that this land-use expansion yield larger nutrient pollution and overcomes the signal derived from technological advances and the pollution reduction policies. This is particularly true for the SSP5-RCP8.5 scenario.

For the regional rivalry scenario SSP3-RCP7.0, results for the North Sea basin show that regional competition and domestic dependencies leads to a decline of population by the end of the century. Reduction of crop, pasture and urban areas implies

https://doi.org/10.5194/egusphere-2024-3645
Preprint. Discussion started: 3 January 2025

that abandoned areas are gradually transformed into natural land (Ma et al., 2020; Hurtt et al., 2020) decreasing the amount of P losses into the rivers (Table 3).

4 Conclusions

This study introduces a novel parameterization to account for total phosphorus (TP) losses in the riverine system at continental and catchment scales. This parameterization was implemented in the HD model. Our results show that the simulated TP losses are consistent in magnitude and trends compared with station measurements. The analysis of 360 global monitoring stations reveals that seasonal fertilizer application practices do not produce a significant seasonal signal in TP concentrations at the catchment scale; only one station showed such a signal. This suggests that P losses derived from seasonal application at agricultural lands are dispersed over time in the riverine system, possibly due to the complex hydrological catchment dynamics. As a result, no seasonal signal was incorporated into our parameterization.

TP load budgets for the four semi-enclosed European seas reveal that small contributions, despite their low value, collectively account for 30% to 60% of the total basin load. This substantial cumulative contribution may explain discrepancies with other modeling studies where such loads may be potentially neglected.

While past efforts to implement pollution reduction policies have successfully reduced nutrient inputs into riverine systems, the future trajectory of human development—and its environmental consequences—remains uncertain. Long-term projections of TP losses indicate that their contribution to eutrophication in European semi-enclosed seas varies significantly across scenarios. While the SSP narratives suggest negative trends in TP loads in the southern European seas, driven by reductions in precipitation, trends substantially differ in the northern seas, particularly for the North Sea; notably, the SSP1-RCP2.6 and SSP5-RCP8.5 scenarios project an increase in nutrient pollution, driven by population growth, land-use changes and increase of precipitation, surpassing the response from advances in technology and pollution reduction measures. Conversely, the SSP3-RCP7.0 scenario for the North Sea, predicts a TP losses decrease due to the decline of population, which subsequently leads to reduced agricultural and urban areas. Such dynamics highlight the complex interactions between climate change, human activity alterations, and nutrient cycling in these regions.

Our simulations and new parameterization can also serve as a valuable resource for providing forcing data to marine ecosystem or Earth system models to improve understanding of the impact of human activities on marine ecosystems.

Data availability. The total phosphorus data from the simulations are available at the World Data Center for Climate repository (Elizalde and Hagemann, 2024).

Author contributions. This study was conceptualized by A.E. and S.H., with data curation, formal analysis, investigation, methodology, software, validation and visualization carried out by A.E. Resources were provided by G.R.M., T.S. and S.H. The original draft was written by A.E., with subsequent review and editing by G.R.M, T.S. and S.H. Project administration and funding acquisition were led by S.H.

https://doi.org/10.5194/egusphere-2024-3645
Preprint. Discussion started: 3 January 2025

Competing interests. The authors declare no conflicts of interest.

395 *Acknowledgements.* This work was supported by the Cluster of Excellence "Climate, Climatic Change, and Society" (CLICCS), project No 390683824, funded by the Deutsche Forschungsgemeinschaft (DFG, German Research Foundation) under Germany's Excellence Strategy - EXC 2037. T.S. was supported by the European Research Council (ERC) under the European Union's Horizon 2020 research and innovation program (grant agreement No 951288, Q-Arctic). Computational resources were made available by the German Climate Computing Center (DKRZ) through support from the German Federal Ministry of Education and Research (BMBF). We gratefully acknowledge the University 400 of Hamburg for providing the data used in this study as part of the GLOWACHEM project, a component in the CLICCS framework.

https://doi.org/10.5194/egusphere-2024-3645
Preprint. Discussion started: 3 January 2025

References

Land-Use Harmonization 2, https://luh.umd.edu/data.shtml, 2018.

Agency, U. E.: Water Information Management System (WIMS), Data retrieved upon request from https://www.gov.uk/, accessed on 28 April 2016, 2016.

Alewell, C., Ringeval, B., Ballabio, C., Robinson, D. A., Panagos, P., and Borrelli, P.: Global phosphorus shortage will be aggravated by soil erosion, Nature Communications, 11, https://doi.org/10.1038/s41467-020-18326-7, 2020.

Bayad, M., Chau, H. W., Trolove, S., Moir, J., Condron, L., and El Gharous, M.: Surface runoff and losses of phosphorus from hydrophobic pastoral soils, Agriculture, Ecosystems and Environment, 324, 107 690, https://doi.org/10.1016/j.agee.2021.107690, 2022.

Behrendt, H., Bach, M., Opitz, D., Pagenkopf, W.-G., Scholz, G., and Wendland, F.: Nutrient Emissions into River Basins of Germany on the Basis of a Harmonized Procedure, Umweltbundesamt, https://www.umweltbundesamt.de/publikationen/nutrient-emissions-into-river-basins-of-germany-on, 221, 2003.

Berthold, M., Wulff, R., Reiff, V., Karsten, U., Nausch, G., and Schumann, R.: Magnitude and influence of atmospheric phosphorus deposition on the southern Baltic Sea coast over 23 years: implications for coastal waters, 31, https://doi.org/10.1186/s12302-019-0208-y, 2019.

Beusen, A. H. W., Beek, L. P. H. V., Bouwman, A. F., Mogollón, J. M., and Middelburg, J. J.: Coupling global models for hydrology and nutrient loading to simulate nitrogen and phosphorus retention in surface water – description of IMAGE–GNM and analysis of performance, Geoscientific Model Development, 8, 4045–4067, https://doi.org/10.5194/gmd-8-4045-2015, 2015.

Beusen, A. H. W., Bouwman, A. F., Beek, L. P. H. V., Mogollón, J. M., and Middelburg, J. J.: Global riverine N and P transport to ocean increased during the 20th century despite increased retention along the aquatic continuum, Biogeosciences, 13, 2441–2451, https://doi.org/10.5194/bg-13-2441-2016, 2016.

BfG: Water quality data. The German Federal Institute of Hydrology (BfG), Retrieved from https://www.bafg.de, accessed on 01 January 2021, 2021.

Bouwman, L., Goldewijk, K. K., Hoek, K. W. V. D., Beusen, A. H. W., Vuuren, D. P. V., Willems, J., Rufino, M. C., and Stehfest, E.: Exploring global changes in nitrogen and phosphorus cycles in agriculture induced by livestock production over the 1900-2050 period, Proceedings of the National Academy of Sciences, 110, 20 882–20 887, https://doi.org/10.1073/pnas.1012878108, 2011.

Calvin, K., Dasgupta, D., Krinner, G., Mukherji, A., Thorne, P. W., Trisos, C., Romero, J., Aldunce, P., Barrett, K., Blanco, G., Cheung, W. W., Connors, S., Denton, F., Diongue-Niang, A., Dodman, D., Garschagen, M., Geden, O., Hayward, B., Jones, C., Jotzo, F., Krug, T., Lasco, R., Lee, Y.-Y., Masson-Delmotte, V., Meinshausen, M., Mintenbeck, K., Mokssit, A., Otto, F. E., Pathak, M., Pirani, A., Poloczanska, E., Pörtner, H.-O., Revi, A., Roberts, D. C., Roy, J., Ruane, A. C., Skea, J., Shukla, P. R., Slade, R., Slangen, A., Sokona, Y., Sörensson, A. A., Tignor, M., van Vuuren, D., Wei, Y.-M., Winkler, H., Zhai, P., Zommers, Z., Hourcade, J.-C., Johnson, F. X., Pachauri, S., Simpson, N. P., Singh, C., Thomas, A., Totin, E., Alegría, A., Armour, K., Bednar-Friedl, B., Blok, K., Cissé, G., Dentener, F., Eriksen, S., Fischer, E., Garner, G., Guivarch, C., Haasnoot, M., Hansen, G., Hauser, M., Hawkins, E., Hermans, T., Kopp, R., Leprince-Ringuet, N., Lewis, J., Ley, D., Ludden, C., Niamir, L., Nicholls, Z., Some, S., Szopa, S., Trewin, B., van der Wijst, K.-I., Winter, G., Witting, M., Birt, A., and Ha, M.: IPCC, 2023: Climate Change 2023: Synthesis Report. Contribution of Working Groups I, II and III to the Sixth Assessment Report of the Intergovernmental Panel on Climate Change [Core Writing Team, H. Lee and J. Romero (eds.)]. IPCC, Geneva, Switzerland., Intergovernmental Panel on Climate Change (IPCC), https://doi.org/10.59327/ipcc/ar6-9789291691647, 2023.

https://doi.org/10.5194/egusphere-2024-3645
Preprint. Discussion started: 3 January 2025

Comission, E.: Report 15: Fertilizers in the EU. DG Agriculture and Rural Development, Unit Analysis and outlook, https://ec.europa.eu/info/food-farming-fisheries/farming/facts-and-figures/performance-agricultural-policy/studies-and-reports/market-analyses-and-briefs_en, 2019.

Compo, G. P., Whitaker, J. S., Sardeshmukh, P. D., Matsui, N., Allan, R. J., Yin, X., Gleason, B. E., Vose, R. S., Rutledge, G., Bessemoulin, P., Brönnimann, S., Brunet, M., Crouthamel, R. I., Grant, A. N., Groisman, P. Y., Jones, P. D., Kruk, M. C., Kruger, A. C., Marshall, G. J., Maugeri, M., Mok, H. Y., Nordli, O., Ross, T. F., Trigo, R. M., Wang, X. L., Woodruff, S. D., and Worley, S. J.: The Twentieth Century Reanalysis Project, Quarterly Journal of the Royal Meteorological Society, 137, 1–28, https://doi.org/10.1002/qj.776, 2011.

Devlin, M. and Brodie, J.: Nutrients and Eutrophication, pp. 75–100, Springer Nature Switzerland, ISBN 9783031101274, https://doi.org/10.1007/978-3-031-10127-4_4, 2023.

Dirmeyer, P. A., Gao, X., Zhao, M., Guo, Z., Oki, T., and Hanasaki, N.: GSWP-2: Multimodel Analysis and Implications for Our Perception of the Land Surface, Bulletin of the American Meteorological Society, 87, 1381–1398, https://doi.org/10.1175/bams-87-10-1381, 2006.

Donnelly, C., Andersson, J. C., and Arheimer, B.: Using flow signatures and catchment similarities to evaluate the E-HYPE multi-basin model across Europe, Hydrological Sciences Journal, 61, 255–273, https://doi.org/10.1080/02626667.2015.1027710, 2015.

EEA: Waterbase - Water Quality, European Environment Agency (EEA), Retrieved from http://www.eea.europa.eu, accessed on 14 February 2022, 2022.

Ekholm, P., Turtola, E., Grönroos, J., Seuri, P., and Ylivainio, K.: Phosphorus loss from different farming systems estimated from soil surface phosphorus balance, Agriculture, Ecosystems & Environment, 110, 266–278, https://doi.org/10.1016/j.agee.2005.04.014, 2005.

Elbe, F.: Das Fachinformationssystem (FIS). Flussgebietsgemeinschaft Elbe (FGG Elbe), Retrieved upon request from www.fgg-elbe.de, accessed on 26 February 2021, 2021.

Elizalde, A. and Hagemann, S.: Total phosphorus transport and river runoff over Europe, World Data Center for Climate (WDCC) at DKRZ. https://doi.org/10.26050/WDCC/cD_Priver_Eur, https://doi.org/10.26050/WDCC/CD_PRIVER_EUR, 2024.

Eyring, V., Bony, S., Meehl, G. A., Senior, C. A., Stevens, B., Stouffer, R. J., and Taylor, K. E.: Overview of the Coupled Model Intercomparison Project Phase 6 (CMIP6) experimental design and organization, Geoscientific Model Development, 9, 1937–1958, https://doi.org/10.5194/gmd-9-1937-2016, 2016.

Gehlot, S., Riddick, T., Hagemann, S., and Brovkin, V.: Implementation of riverine organic carbon transport into the land surface model JSBACH: technical report, https://doi.org/10.17617/2.3602778, 2024.

Gupta, H. V., Kling, H., Yilmaz, K. K., and Martinez, G. F.: Decomposition of the mean squared error and NSE performance criteria: Implications for improving hydrological modelling, Journal of Hydrology, 377, 80–91, https://doi.org/10.1016/j.jhydrol.2009.08.003, 2009.

Gustafsson, B. G., Schenk, F., Blenckner, T., Eilola, K., Meier, H. E. M., Müller-Karulis, B., Neumann, T., Ruoho-Airola, T., Savchuk, O. P., and Zorita, E.: Reconstructing the Development of Baltic Sea Eutrophication 1850–2006, AMBIO, 41, 534–548, https://doi.org/10.1007/s13280-012-0318-x, 2012.

Hagemann, S. and Stacke, T.: Complementing ERA5 and E-OBS with high-resolution river discharge over Europe, Oceanologia, 65, 230–248, https://doi.org/10.1016/j.oceano.2022.07.003, 2023.

Hagemann, S., Stacke, T., and Ho-Hagemann, H. T. M.: High Resolution Discharge Simulations Over Europe and the Baltic Sea Catchment, Frontiers in Earth Science, 8, https://doi.org/10.3389/feart.2020.00012, 2020.

Hart, M. R., Quin, B. F., and Nguyen, M. L.: Phosphorus Runoff from Agricultural Land and Direct Fertilizer Effects: A Review, Journal of Environmental Quality, 33, 1954–1972, https://doi.org/10.2134/jeq2004.1954, 2004.

https://doi.org/10.5194/egusphere-2024-3645
Preprint. Discussion started: 3 January 2025

Hartmann, J. and Moosdorf, N.: Chemical weathering rates of silicate-dominated lithological classes and associated liberation rates of phosphorus on the Japanese Archipelago—Implications for global scale analysis, Chemical Geology, 287, 125–157, https://doi.org/10.1016/j.chemgeo.2010.12.004, 2011.

Hartmann, J., Lauerwald, R., and Moosdorf, N.: A Brief Overview of the GLObal RIver Chemistry Database, GLORICH, 10, 23–27, https://doi.org/10.1016/j.proeps.2014.08.005, 2014a.

Hartmann, J., Moosdorf, N., Lauerwald, R., Hinderer, M., and West, A. J.: Global chemical weathering and associated P-release — The role of lithology, temperature and soil properties, Chemical Geology, 363, 145–163, https://doi.org/10.1016/j.chemgeo.2013.10.025, 2014b.

HELCOM: Baltic Sea Action Plan, https://helcom.fi/baltic-sea-action-plan/, 2007.

Hua, K. and Zhu, B.: Phosphorus loss through surface runoff and leaching in response to the long-term application of different organic amendments on sloping croplands, Journal of Soils and Sediments, 20, 3459–3471, https://doi.org/10.1007/s11368-020-02675-3, 2020.

Hurtt, G. C., Chini, L., Sahajpal, R., Frolking, S., Bodirsky, B. L., Calvin, K., Doelman, J. C., Fisk, J., Fujimori, S., Goldewijk, K. K., Hasegawa, T., Havlik, P., Heinimann, A., Humpenöder, F., Jungclaus, J., Kaplan, J., Kennedy, J., Kristzin, T., Lawrence, D., Lawrence, P., Ma, L., Mertz, O., Pongratz, J., Popp, A., Poulter, B., Riahi, K., Shevliakova, E., Stehfest, E., Thornton, P., Tubiello, F. N., van Vuuren, D. P., and Zhang, X.: Harmonization of Global Land-Use Change and Management for the Period 850–2100 (LUH2) for CMIP6, https://doi.org/10.5194/gmd-2019-360, 2020.

Hyndman, R. J. and Athanasopoulos, G.: Forecasting: principles and practice, 2nd edition, OTexts: Melbourne, Australia. OTexts.com/fpp2., https://otexts.com/fpp2/, 2018.

ICN: International Conference on the Protection of the North Sea, 1987.

Iglesias, I., Buschman, F., Simone, G., Amorim, F., Bio, A., Vieira, L., Boisgontier, H., Zaggia, L., Moschino, V., Madricardo, F., Sousa-Pinto, I., and Antunes, S.: Hydrodynamics of a highly stratified small estuary and the influence of nearby river plumes, Estuarine, Coastal and Shelf Science, 304, 108 843, https://doi.org/10.1016/j.ecss.2024.108843, 2024.

John, J. G., Blanton, C., McHugh, C., Radhakrishnan, A., Rand, K., Vahlenkamp, H., Wilson, C., Zadeh, N. T., Dunne, J. P., Dussin, R., Horowitz, L. W., Krasting, J. P., Lin, P., Malyshev, S., Naik, V., Ploshay, J., Shevliakova, E., Silvers, L., Stock, C., Winton, M., and Zeng, Y.: NOAA-GFDL GFDL-ESM4 model output prepared for CMIP6 ScenarioMIP, https://doi.org/10.22033/ESGF/CMIP6.1414, 2018.

KC, S. and Lutz, W.: The human core of the shared socioeconomic pathways: Population scenarios by age, sex and level of education for all countries to 2100, 42, 181–192, https://doi.org/10.1016/j.gloenvcha.2014.06.004, 2017.

Kempe, S.: Long-term records of CO2 pressure fluctuations in fresh waters, SCOPE/UNEP Sonderband, 52, 91–332, 1982.

Kim, H.: Global Soil Wetness Project Phase 3 Atmospheric Boundary Conditions (Experiment 1). Data Integration and Analysis System (DIAS)., https://doi.org/10.20783/DIAS.501, 2017.

Kjellström, E., Nikulin, G., Hansson, U., Strandberg, G., and Ullerstig, A.: 21st century changes in the European climate: uncertainties derived from an ensemble of regional climate model simulations, Tellus A: Dynamic Meteorology and Oceanography, 63, 24, https://doi.org/10.1111/j.1600-0870.2010.00475.x, 2011.

Kling, H., Fuchs, M., and Paulin, M.: Runoff conditions in the upper Danube basin under an ensemble of climate change scenarios, Journal of Hydrology, 424–425, 264–277, https://doi.org/10.1016/j.jhydrol.2012.01.011, 2012.

Knoben, W. J. M., Freer, J. E., and Woods, R. A.: Technical note: Inherent benchmark or not? Comparing Nash–Sutcliffe and Kling–Gupta efficiency scores, Hydrology and Earth System Sciences, 23, 4323–4331, https://doi.org/10.5194/hess-23-4323-2019, 2019.

Kovats, R., Valentini, R., Bouwer, L., Georgopoulou, E., Jacob, D., Martin, E., Rounsevell, M., and Soussana, J.-F.: Europe. In: Climate Change 2014: Impacts, Adaptation, and Vulnerability. Part B: Regional Aspects.Contribution of Working Group II to the Fifth Assessment

https://doi.org/10.5194/egusphere-2024-3645
Preprint. Discussion started: 3 January 2025

Report of the Intergovernmental Panel on ClimateChange [Barros, V.R., C.B. Field, D.J. Dokken, M.D. Mastrandrea, K.J. Mach, T.E. Bilir, M. Chatterjee, K.L. Ebi,Y.O. Estrada, R.C. Genova, B. Girma, E.S. Kissel, A.N. Levy, S. MacCracken, P.R. Mastrandrea, and L.L. White(eds.)]., Fifth Assessment Report of the Intergovernmental Panel on ClimateChange, Cambridge University Press, Cambridge, United Kingdom and New York, NY, USA., pp. 1267–1326, https://www.ipcc.ch/report/ar5/wg2/, 2014.

Kronvang, B., Vagstad, N., Behrendt, H., Bøgestrand, J., and Larsen, S. E.: Phosphorus losses at the catchment scale within Europe: an overview, Soil Use and Management, 23, 104–116, https://doi.org/10.1111/j.1475-2743.2007.00113.x, 2007.

Lange, S. and Büchner, M.: ISIMIP3b bias-adjusted atmospheric climate input data, https://doi.org/10.48364/ISIMIP.842396.1, 2021.

Lee, K. Y., van Geldern, R., and Barth, J. A.: A high-resolution carbon balance in a small temperate catchment: Insights from the Schwabach River, Germany, Applied Geochemistry, 85, 86–96, https://doi.org/10.1016/j.apgeochem.2017.08.007, 2017.

LfU: Fließgewässer. Bayerisches Landesamt für Umwelt (LfU), Available upon request from www.lfu.bayern.de, accessed on 07 December 2017, 2017.

Liu, W., Ciais, P., Liu, X., Yang, H., Hoekstra, A. Y., Tang, Q., Wang, X., Li, X., and Cheng, L.: Global Phosphorus Losses from Croplands under Future Precipitation Scenarios, Environmental Science & Technology, 54, 14 761–14 771, https://doi.org/10.1021/acs.est.0c03978, 2020.

Lun, F., Liu, J., Ciais, P., Nesme, T., Chang, J., Wang, R., Goll, D., Sardans, J., Peñuelas, J., and Obersteiner, M.: Global and regional phosphorus budgets in agricultural systems and their implications for phosphorus-use efficiency, Earth System Science Data, 10, 1–18, https://doi.org/10.5194/essd-10-1-2018, 2018.

Ma, L., Hurtt, G. C., Chini, L. P., Sahajpal, R., Pongratz, J., Frolking, S., Stehfest, E., Klein Goldewijk, K., O'Leary, D., and Doelman, J. C.: Global rules for translating land-use change (LUH2) to land-cover change for CMIP6 using GLM2, Geoscientific Model Development, 13, 3203–3220, https://doi.org/10.5194/gmd-13-3203-2020, 2020.

Mitter, H., Techen, A.-K., Sinabell, F., Helming, K., Schmid, E., Bodirsky, B. L., Holman, I., Kok, K., Lehtonen, H., Leip, A., Le Mouël, C., Mathijs, E., Mehdi, B., Mittenzwei, K., Mora, O., Øistad, K., Øygarden, L., Priess, J. A., Reidsma, P., Schaldach, R., and Schönhart, M.: Shared Socio-economic Pathways for European agriculture and food systems: The Eur-Agri-SSPs, Global Environmental Change, 65, 102 159, https://doi.org/10.1016/j.gloenvcha.2020.102159, 2020.

Mogollón, J., Beusen, A., van Grinsven, H., Westhoek, H., and Bouwman, A.: Future agricultural phosphorus demand according to the shared socioeconomic pathways, Global Environmental Change, 50, 149–163, https://doi.org/10.1016/j.gloenvcha.2018.03.007, 2018.

Mogollón, J. M., Bouwman, A. F., Beusen, A. H. W., Lassaletta, L., van Grinsven, H. J. M., and Westhoek, H.: More efficient phosphorus use can avoid cropland expansion, Nature Food, 2, 509–518, https://doi.org/10.1038/s43016-021-00303-y, 2021.

Motesharezadeh, B., Etesami, H., Bagheri-Novair, S., and Amirmokri, H.: Fertilizer consumption trend in developing countries vs. developed countries, Environmental Monitoring and Assessment, 189, https://doi.org/10.1007/s10661-017-5812-y, 2017.

Olarewaju, O. E., Adetunji, M. T., Adeofun, C. O., and Adekunle, I. M.: Nitrate and phosphorus loss from agricultural land: implications for nonpoint pollution, Nutrient Cycling in Agroecosystems, 85, 79–85, https://doi.org/10.1007/s10705-009-9249-8, 2009.

O'Neill, B. C., Kriegler, E., Ebi, K. L., Kemp-Benedict, E., Riahi, K., Rothman, D. S., van Ruijven, B. J., van Vuuren, D. P., Birkmann, J., Kok, K., Levy, M., and Solecki, W.: The roads ahead: Narratives for shared socioeconomic pathways describing world futures in the 21st century, Global Environmental Change, 42, 169–180, https://doi.org/10.1016/j.gloenvcha.2015.01.004, 2017.

Programme, U. N. E.: GEMStat database of theGlobal Environment Monitoring System for Freshwater (GEMS/Water) Programme. International Centre for Water Resources and Global Change, Koblenz, Available upon request from GEMS/Water Data Centre: gemstat.org, 2019.

https://doi.org/10.5194/egusphere-2024-3645
Preprint. Discussion started: 3 January 2025

Raudsepp, U., Maljutenko, I., Barzandeh, A., Uiboupin, R., and Lagemaa, P.: Baltic Sea freshwater content, State of the Planet, 1-osr7, 7, https://doi.org/10.5194/sp-1-osr7-7-2023, 2023.

Riahi, K., van Vuuren, D. P., Kriegler, E., Edmonds, J., O'Neill, B. C., Fujimori, S., Bauer, N., Calvin, K., Dellink, R., Fricko, O., Lutz, W., Popp, A., Cuaresma, J. C., KC, S., Leimbach, M., Jiang, L., Kram, T., Rao, S., Emmerling, J., Ebi, K., Hasegawa, T., Havlik, P., Humpenöder, F., Silva, L. A. D., Smith, S., Stehfest, E., Bosetti, V., Eom, J., Gernaat, D., Masui, T., Rogelj, J., Strefler, J., Drouet, L., Krey, V., Luderer, G., Harmsen, M., Takahashi, K., Baumstark, L., Doelman, J. C., Kainuma, M., Klimont, Z., Marangoni, G., Lotze-Campen, H., Obersteiner, M., Tabeau, A., and Tavoni, M.: The Shared Socioeconomic Pathways and their energy, land use, and greenhouse gas emissions implications: An overview, Global Environmental Change, 42, 153–168, https://doi.org/10.1016/j.gloenvcha.2016.05.009, 2017.

Ritchie, J. and Dowlatabadi, H.: Why do climate change scenarios return to coal?, Energy, 140, 1276–1291, https://doi.org/10.1016/j.energy.2017.08.083, 2017.

SEFARI: National waters inventory for scotland. Scottish Environment, Food and Agricultural Research Institutes (SEFARI), Retrieved from http://nar.hutton.ac.uk, accessed on 21 August 2020, 2020.

Senay, G. B., Velpuri, N. M., Bohms, S., Demissie, Y., and Gebremichael, M.: Understanding the hydrologic sources and sinks in the Nile Basin using multisource climate and remote sensing data sets, Water Resources Research, 50, 8625–8650, https://doi.org/10.1002/2013wr015231, 2014.

Smith, V. H., Joye, S. B., and Howarth, R. W.: Eutrophication of freshwater and marine ecosystems, Limnology and Oceanography, 51, 351–355, https://doi.org/10.4319/lo.2006.51.1_part_2.0351, 2006.

Stacke, T. and Hagemann, S.: HydroPy and MPI-HM simulation data driven with GSWP3 meteorological forcing, https://doi.org/10.26050/WDCC/HydroPy_MPI-HM_hist_sim, 2021.

Stehfest, E., van Zeist, W.-J., Valin, H., Havlik, P., Popp, A., Kyle, P., Tabeau, A., Mason-D'Croz, D., Hasegawa, T., Bodirsky, B. L., Calvin, K., Doelman, J. C., Fujimori, S., Humpenöder, F., Lotze-Campen, H., van Meijl, H., and Wiebe, K.: Key determinants of global land-use projections, 10, https://doi.org/10.1038/s41467-019-09945-w, 2019.

Svendsen, L. M. and Gustafsson, B.: Waterborne nitrogen and phosphorus inputs and water flow to the BalticSea 1995-2021, Tech. rep., Baltic Marine Environment Protection Commission, https://helcom.fi/baltic-sea-trends/environment-fact-sheets/eutrophication/, 2023.

Tipping, E., Benham, S., Boyle, J. F., Crow, P., Davies, J., Fischer, U., Guyatt, H., Helliwell, R., Jackson-Blake, L., Lawlor, A. J., Monteith, D. T., Rowe, E. C., and Toberman, H.: Atmospheric deposition of phosphorus to land and freshwater, Environ. Sci.: Processes Impacts, 16, 1608–1617, https://doi.org/10.1039/c3em00641g, 2014.

van Geldern, R., Schulte, P., Mader, M., Baier, A., and Barth, J. A.: Spatial and temporal variations of pCO2, dissolved inorganic carbon and stable isotopes along a temperate karstic watercourse, Hydrological Processes, 29, 3423–3440, https://doi.org/10.1002/hyp.10457, 2015.

van Geldern, R., Schulte, P., Mader, M., Baier, A., Barth, J. A., Juhlke, T. R., and Lee, K.: Insights into agricultural influences and weathering processes from major ion patterns, Hydrological Processes, 32, 891–903, https://doi.org/10.1002/hyp.11461, 2018.

van Vuuren, D. P., Stehfest, E., den Elzen, M. G. J., Kram, T., van Vliet, J., Deetman, S., Isaac, M., Klein Goldewijk, K., Hof, A., Mendoza Beltran, A., Oostenrijk, R., and van Ruijven, B.: RCP2.6: exploring the possibility to keep global mean temperature increase below 2°C, Climatic Change, 109, 95–116, https://doi.org/10.1007/s10584-011-0152-3, 2011.

van Vuuren, D. P., Stehfest, E., Gernaat, D. E., Doelman, J. C., van den Berg, M., Harmsen, M., de Boer, H. S., Bouwman, L. F., Daioglou, V., Edelenbosch, O. Y., Girod, B., Kram, T., Lassaletta, L., Lucas, P. L., van Meijl, H., Müller, C., van Ruijven, B. J., van der Sluis, S., and

https://doi.org/10.5194/egusphere-2024-3645
Preprint. Discussion started: 3 January 2025

Tabeau, A.: Energy, land-use and greenhouse gas emissions trajectories under a green growth paradigm, Global Environmental Change, 42, 237–250, https://doi.org/10.1016/j.gloenvcha.2016.05.008, 2017.

Wang, X., Smith, K., and Hyndman, R.: Characteristic-Based Clustering for Time Series Data, 13, 335–364, https://doi.org/10.1007/s10618-005-0039-x, 2006.

Warszawski, L., Frieler, K., Huber, V., Piontek, F., Serdeczny, O., and Schewe, J.: The Inter-Sectoral Impact Model Intercomparison Project (ISI–MIP): Project framework, Proceedings of the National Academy of Sciences, 111, 3228–3232, https://doi.org/10.1073/pnas.1312330110, 2013.

Yuan, Z., Jiang, S., Sheng, H., Liu, X., Hua, H., Liu, X., and Zhang, Y.: Human Perturbation of the Global Phosphorus Cycle: Changes and Consequences, Environmental Science and Technology, 52, 2438–2450, https://doi.org/10.1021/acs.est.7b03910, 2018.